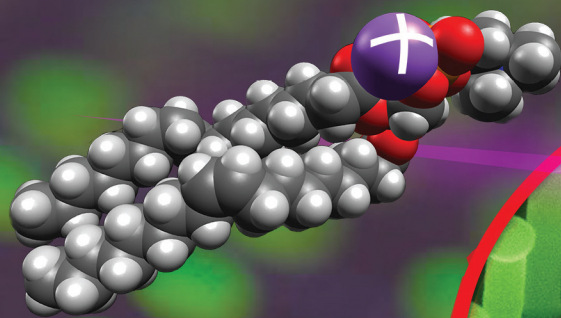
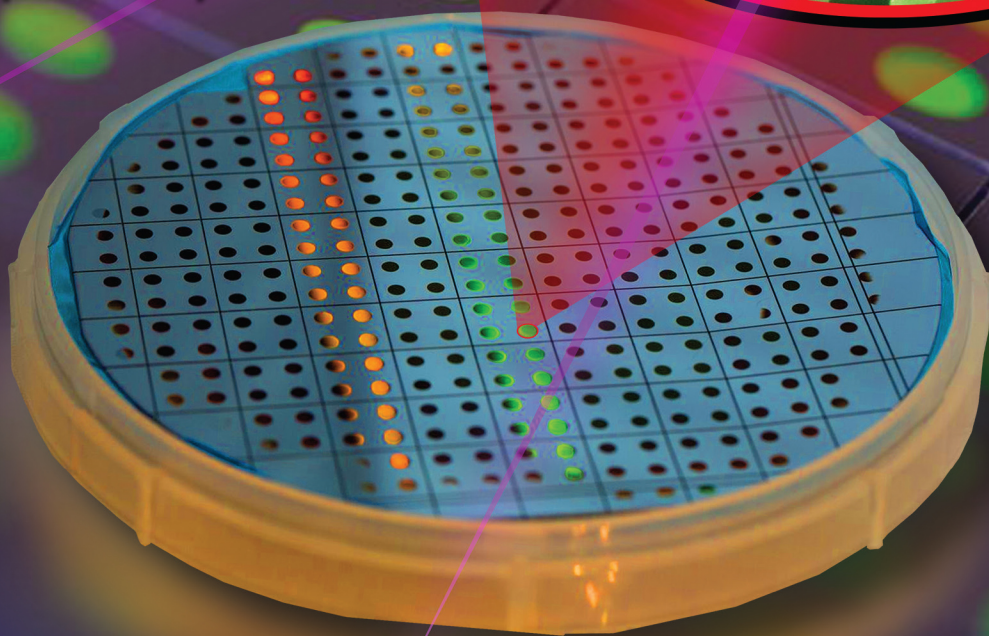
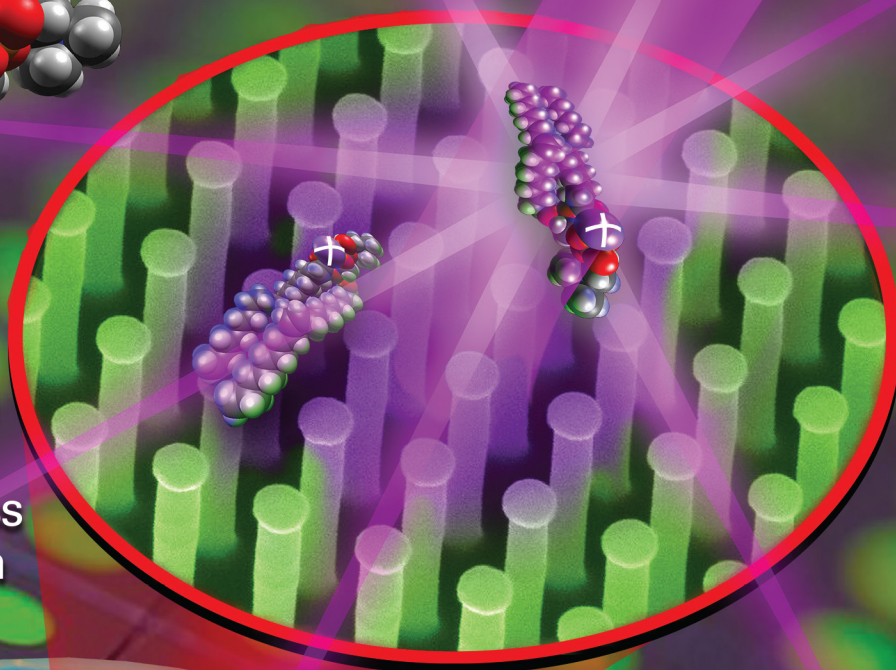


analytical chemistry

September 20, 2016 Volume 88 Number 18



Large-Scale Metabolite
Analysis of Standards and
Human Serum by Laser
Desorption Ionization Mass
Spectrometry from Silicon
Nanopost Arrays



Large-Scale Metabolite Analysis of Standards and Human Serum by Laser Desorption Ionization Mass Spectrometry from Silicon Nanopost Arrays

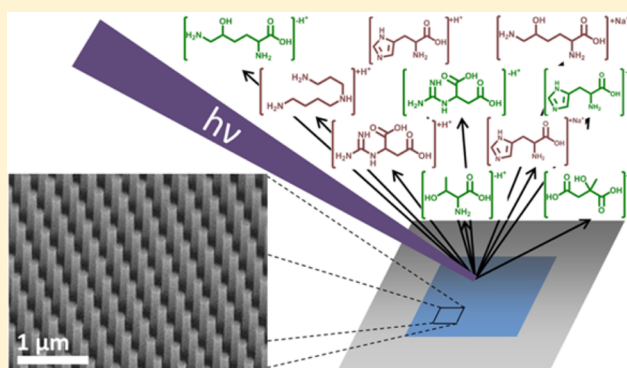
Andrew R. Korte,[†] Sylwia A. Stopka,[†] Nicholas Morris,[‡] Trust Razunguzwa,[‡] and Akos Vertes^{*,†}

[†]Department of Chemistry, George Washington University, 800 22nd Street, North West, Washington, District of Columbia 20052, United States

[‡]Protea Biosciences, Inc., Morgantown, West Virginia 26505, United States

S Supporting Information

ABSTRACT: The unique challenges presented by metabolomics have driven the development of new mass spectrometry (MS)-based techniques for small molecule analysis. We have previously demonstrated silicon nanopost arrays (NAPA) to be an effective substrate for laser desorption ionization (LDI) of small molecules for MS. However, the utility of NAPA-LDI-MS for a wide range of metabolite classes has not been investigated. Here we apply NAPA-LDI-MS to the large-scale acquisition of high-resolution mass spectra and tandem mass spectra from a collection of metabolite standards covering a range of compound classes including amino acids, nucleotides, carbohydrates, xenobiotics, lipids, and other classes. In untargeted analysis of metabolite standard mixtures, detection was achieved for 374 compounds and useful MS/MS spectra were obtained for 287 compounds, without individual optimization of ionization or fragmentation conditions. Metabolite detection was evaluated in the context of 31 metabolic pathways, and NAPA-LDI-MS was found to provide detection for 63% of investigated pathway metabolites. Individual, targeted analysis of the 20 common amino acids provided detection of 100% of the investigated compounds, demonstrating that improved coverage is possible through optimization and targeting of individual analytes or analyte classes. In direct analysis of aqueous and organic extracts from human serum samples, spectral features were assigned to a total of 108 small metabolites and lipids. Glucose and amino acids were quantitated within their physiological concentration ranges. The broad coverage demonstrated by this large-scale screening experiment opens the door for use of NAPA-LDI-MS in numerous metabolite analysis applications.



In comparison to proteomics and transcriptomics, metabolomics is a less developed field. Where complete or near-complete molecular coverage has been achieved in genomics,¹ transcriptomics,² and proteomics,³ there is no consensus general method for large-scale metabolomics. Although progress has been made toward global metabolomics measurements,^{4,5} these efforts are hampered by the wide concentration range, diverse chemical functionality, and isomeric complexity of cellular metabolites. The search for a global, sensitive metabolomics methodology has largely focused on mass spectrometry (MS) due to its wide applicability, high specificity, and ability to provide significant chemical information about analytes.

Most MS-based metabolomics experiments make use of electrospray ionization (ESI). While ESI can be readily coupled to separation techniques such as liquid chromatography and capillary electrophoresis, the need to dissolve the sample in an ESI-compatible solvent system can limit its applicability, especially for nonpolar analytes. Moreover, the generation of solvent adducts and multiply charged species, often beneficial

for higher-mass analysis, can lead to undesirable complications of low-mass spectra.

One alternative to ESI-MS is laser desorption ionization (LDI)-MS, most commonly matrix-assisted laser desorption ionization (MALDI). However, using MALDI for metabolomics presents several additional challenges. The small organic molecules used as matrixes in MALDI-MS can lead to spectral interferences. Different classes of metabolites often require the use of different matrixes. For MS imaging of metabolites, the uniformity of the deposited matrix can result in further complications. To alleviate these problems, a number of alternative laser desorption/ionization techniques have been developed based on nanostructured surfaces, including desorption ionization on silicon (DIOS),⁶ laser-induced silicon microcolumn arrays (LISMA),⁷ and nanostructure initiator

Received: March 25, 2016

Accepted: July 11, 2016

Published: July 11, 2016

mass spectrometry (NIMS).⁸ Other nanomaterials utilized for LDI include nanowires^{9,10} and nanoparticles.^{11–14} These alternative techniques are particularly advantageous for metabolomics applications, where the low-mass background from MALDI matrixes can interfere with the analytes of interest.

Silicon nanopost arrays (NAPA) have also been shown to be effective nanophotonic platforms for LDI, allowing rapid, sensitive analysis, often with minimal sample preparation.^{15–18} Although the NAPA-LDI experimental arrangement is similar to matrix-assisted laser desorption ionization (MALDI),^{11,19,20} the nanophotonic interactions between a NAPA structure and the laser light result in significantly reduced chemical background, enhanced sensitivity, and wide dynamic range.

In NAPA-LDI-MS, silicon nanoposts act as nanoscopic antennas for the absorption and transfer of incident laser energy to the deposited sample material. Precise nanofabrication of these arrays allows for the careful tuning of physical properties through the array geometry (e.g., post diameter and aspect ratio) and optimization of nanophotonic performance.¹⁵ The development of a new production methodology based on deep ultraviolet-projection lithography²¹ has enabled the high-throughput fabrication of these NAPA platforms. The produced chips enabled the quantitation of small molecules, both in prepared solutions, and in urine and serum samples²² with more than 3 orders of magnitude dynamic range and R^2 values of 0.99. More recently, NAPA-LDI-MS has been employed for molecular imaging from tissue sections.²³

Advances in resolving power and sensitivity have greatly expanded the usefulness of mass spectrometry for analysis of complex biological samples in applications such as metabolomics.²⁴ Many high-resolution mass spectrometers are capable of mass accuracies on the order of parts per million (ppm) with or even without internal calibration.²⁵ This high mass accuracy simplifies the assignment of molecular formulas but is often not sufficient for confident assignment of molecular identities to observed ion signals. Even when a molecular formula can be confidently assigned, there are often many isomeric potential identities. By nature, LDI-MS techniques lack chromatographic separation, making verification by other means (e.g., database searching of tandem mass spectra) crucial to confident metabolite identification. Several aggregated databases of MS/MS spectra are available either freely or for purchase, including those provided by the National Institute for Standards and Technology Mass Spectrometry Data Center (<http://www.nist.gov/srd/nist1a.cfm>, last accessed on March 19, 2016) and the Scripps Center for Metabolomics (<https://xmsonline.scripps.edu/>, last accessed on March 19, 2016). These databases, however, rely on conventional ionization methods (e.g., electron impact, ESI, and MALDI) that generate ions with specific internal energies. Additionally, they typically aggregate data from multiple instrumental platforms, isolation/activation techniques, and parameters, but fragmentation spectra can vary widely depending on these conditions.^{26,27} In LDI from NAPA, the internal energies of the ions, and therefore their fragmentation depend on the laser fluence.²⁸ Moreover, as shown in this work, NAPA-LDI can produce ionic species not typically observed in ESI or MALDI. For this reason, here we conduct a large-scale screening of over 600 metabolite standards to assess the ability of NAPA-LDI-MS to analyze a range of metabolically relevant compounds and demonstrate the acquisition of the corresponding tandem mass

spectra from this same large-scale screening. The metabolite standards used here represent numerous molecular classes and metabolic functions, including amino acids, carbohydrates, vitamins, hormones, lipids, nucleosides, and xenobiotics.

■ EXPERIMENTAL SECTION

Chemicals. A collection of 618 small molecule metabolite standards on seven 96-well plates (IROA 300, Mass Spectrometry Metabolite Library of Standards, MSMLS) was purchased from IROA Technologies (Bolton, MA). Water (catalog no. W6), acetonitrile (catalog no. A955), and methanol (catalog no. A456) (all Optima LC–MS grade), and ethanol (catalog no. BP2818, molecular biology grade) were purchased from Fisher Scientific (Pittsburgh, PA). Standards of the 20 proteinogenic L-amino acids, 3',5'-cyclic adenosine monophosphate (cAMP), and acetylcholine chloride were purchased from Sigma-Aldrich (St. Louis, MO).

Nanopost Array Fabrication. Fabrication of silicon nanoposts was achieved using deep ultraviolet projection photolithography (DUV-PL) and deep reactive ion etching (DRIE). Low resistivity (0.001–0.005 Ω cm) $\langle 100 \rangle$ p-type silicon wafers (Silicon Valley Microelectronics, Inc., Santa Clara, CA) were used. An antireflective coating (AR2-600, DOW Shipley, Marlborough, MA) was spin coated on the native silicon surface at 3500 rpm for 30 s and baked on a hot plate at 220 °C for 1 min. Negative-tone DUV photoresist (UVN-2300, DOW Shipley, Marlborough, MA) was then spin-coated at 3500 rpm for 30 s before a bake at 110 °C for 90 s. A 248 nm wavelength lithography stepper system (PAS 5500/300, ASML, Veldhoven, The Netherlands) was used for pattern transfer. After exposure, a 60 s hot plate bake was performed at 105 °C. The photoresist was developed using an agitated bath of AZ300MIF (Clariant, Somerville, NJ) for 60 s, followed by a bath in deionized water for 60 s. Wafers were dried using N_2 gas. The DRIE (PlasmaTherm 790, St. Petersburg, FL) vertical Si etch was performed with a chamber pressure of 19 mTorr, an ICP power of 825 W, and an RIE power of 15 W for 9 min. The mixture of etchant gases was as follows: C_4F_8 (52 sccm), SF_6 (28 sccm), and Ar (20 sccm). Wafers were etched to a depth of 1100 nm. After DRIE, wafers were cleaned using O_2 plasma (Technics PEII, Pleasanton, CA) at 300 mTorr and 100 W for 3 min. The fabrication process resulted in nanoposts with significant surface fluorination due to the presence of C_4F_8 and SF_6 in the ion etching gas mixture.²¹ Final post dimensions were 150 nm in diameter and 1100 nm in height with a periodicity of 337 nm. Nanopost arrays were stored in a desiccator cabinet with cleanroom grade desiccant that provided a low humidity environment until use.

Instrumentation. All spectra in this work were acquired using a MALDI-LTQ-Orbitrap XL mass spectrometer (Thermo Scientific, San Jose, CA). This instrument features an intermediate-pressure (75 mTorr) MALDI source and a nitrogen gas laser emitting 337 nm radiation at a 60 Hz repetition rate. Laser radiation strikes the sample at an angle of 32° to the normal. For analysis, NAPA chips spotted with sample material were affixed to a MALDI sample plate using double-sided carbon tape (Ted Pella, Inc., Redding, CA) and inserted into the mass spectrometer. Unless otherwise noted, spectra were acquired using the orbitrap analyzer at a nominal resolution of 30 000.

Preparation of Standard Mixtures. Each well of the MSMLS plates was filled with 100 μ L of the appropriate solvent (water, 40% (v/v) methanol, or ethanol per the suggestion of

the manufacturer), and the plates were incubated at 4 °C overnight. Mixtures of up to 12 metabolite standards were created by pooling 50 μL of the solutions from the wells in each plate row. For rows with potential interferences (i.e., compounds with nominal masses within a window of ± 1 Da), all of the interfering compounds were omitted from the mixture. The mixtures were then dried in a vacuum centrifuge and reconstituted in 20 μL of the original solvent to arrive to a final concentration range of 9.2×10^{-5} to 2.8×10^{-3} M. A 1.0 μL volume of each solution was deposited by pipetting directly onto two NAPA chips (one each for positive and negative ion mode analysis) and allowed to dry under ambient conditions resulting in a deposited amount ranging from 9.2×10^{-11} to 2.8×10^{-9} moles per compound. As the surfaces are super-hydrophobic, care must be taken that all of the deposited sample remains on the chip surface.

Analysis of Standard Mixtures. Spectra were acquired using the tissue imaging function in the instrument control software. A raster pitch of 75 μm was used in both dimensions. For all acquisitions, one mass spectrum and three tandem mass spectra were acquired from each raster point by splitting the raster point into four steps. At the first step, a high-resolution mass spectrum was collected using the orbitrap analyzer at a resolving power setting of 30 000. Data-dependent tandem mass spectra were collected in 25 μm steps at points 2–4 based on the MS scan in step 1. Using this method, a total of ~ 2500 –3500 scans were collected across the surface of each 4–5 mm^2 sample. All scans were collected using 3 shots/scan at a fluence of 40 mJ/cm^2 . The effect of the laser fluence is further explored in the [Results and Discussion](#).

For tandem MS, ions were isolated with a window of ± 0.75 Th and fragmented at a normalized collision energy of 35 (instrument units), activation q of 0.250, and activation time of 30 ms for all spectra. Fragment ions were analyzed using the ion trap. Data-dependent selection of ions for fragmentation was based on a list of calculated masses generated for each mixture, comprising the $[\text{M} + \text{H}]^+$, $[\text{M} + \text{H} - \text{H}_2\text{O}]^+$, $[\text{M} + \text{Na}]^+$, and $[\text{M} + \text{K}]^+$ species in positive ion mode and $[\text{M} - \text{H}]^-$ and $[\text{M} - \text{H} - \text{H}_2\text{O}]^-$ in negative ion mode. At each raster point, the three most abundant observed ions from this list were subjected to tandem MS. The tolerance for selection of an ion was ± 20 ppm from the calculated mass. To prevent repeated acquisition of spectra from the most abundant ions, the dynamic exclusion function was used, with a repeat count of 2, repeat duration of 60 s, exclusion list size of 50, exclusion duration of 120 s, and exclusion mass width of ± 20 ppm.

Preparation and Analysis of Individual Standards. Standards of cAMP and acetylcholine were dissolved in water and serially diluted to provide a range of concentrations for deposition. For fluence testing, 10^{-9} mol of the standard was deposited onto several NAPA chips and each chip was irradiated at a different fluence. Chips with a 2 mm diameter active area were analyzed using the imaging function in the instrument control software at a raster pitch of 100 μm . After acquisition, the entire scan was averaged and ion intensities were extracted from the averaged spectrum. For quantitative testing of cAMP and acetylcholine, several concentrations were deposited onto different chips, and irradiated at a fluence of 100 mJ/cm^2 . All spectra were collected using 3 laser shots/scan.

Amino acid standards were dissolved in water and 10^{-9} mol of each was deposited onto separate NAPA chips. After acquisition using the method described above, data was imported to ImageQuest software and the six contiguous raster

points providing the highest base peak intensity were averaged. Amino acid-related peaks were identified by accurate mass.

Evaluation of Spectra. After acquisition, spectra were examined using the Xcalibur QualBrowser software (Thermo Scientific, San Jose, CA). High-resolution, accurate mass orbitrap mass spectra were inspected to verify the presence of the ions of interest and to identify any potential interferences. Ion species showing a signal-to-noise ratio of >3 were considered detected. Tandem mass spectra for a given ion were considered diagnostically useful only if the parent ion was detected in orbitrap MS spectra, no significant interferences were detected within ± 1 Th of the m/z of interest, and the base peak intensity of the MS/MS spectrum was at least 200 counts.

Following acquisition and examination, raw data files (*.raw) were imported into Mass Frontier (Thermo Scientific, San Jose, CA). The direct infusion component detection algorithm was used to identify and extract tandem MS scans from the data-dependent acquisitions. For those ions meeting the above criteria, MS/MS spectra were imported and stored. The assignment of molecular structures and ion species allowed for the pairing of MS/MS spectra with calculated exact masses.

RESULTS AND DISCUSSION

Metabolite Coverage. [Figures 1](#) and [2](#) present sample spectra obtained from positive and negative ion mode analysis, respectively, of a prepared mixture of 11 metabolite standards. High-resolution MS scans allowed for the confirmation of ion identities and the identification of any potential interferences that might hinder MS/MS analysis. Proposed fragmentation schemes are presented for the purpose of illustration but were not assigned for all acquired MS/MS spectra.

A summary of the overall coverage of metabolite standards for the given conditions is provided in [Table 1](#) and [Table 2](#) for positive and negative ion modes, respectively. A total of 501 diagnostically useful tandem MS spectra were obtained (251 in positive ion mode and 250 in negative ion mode). An additional 459 ions were detected in MS spectra but did not provide diagnostically useful tandem MS spectra. Tandem MS spectra were acquired for at least one ionic form in at least one polarity for 287 out of 618 compounds (46% coverage) under the set of selected conditions (i.e., metabolite pooling, laser fluence, and collision energy). An additional 87 compounds were detected by MS in at least one ionic form in at least one polarity but did not provide diagnostically useful MS/MS spectra. Thus, in total 374 metabolites were detected in at least one ionic form for a metabolite coverage of 61%. A full listing of detected metabolite standards, including the detected ionic species, is provided in [Spreadsheet S1](#) in the Supporting Information.

For 134 compounds in positive mode and 46 compounds in negative mode, precursor ions were detected in MS scans but useful MS/MS spectra were not obtained. For some ions, this was due to interferences from similar m/z ions that prevented adequate isolation of the ion of interest prior to fragmentation. For other compounds, no interfering ions were observed but the acquired MS/MS spectra did not show significant fragment ion intensity, either due to low precursor abundance or poor yields of stable fragments.

Postacquisition analysis of high-resolution MS spectra revealed that a number of compounds yielded significant ion abundances for the $[\text{M} + 2\text{Na} - \text{H}]^+$ and $[\text{M} + 2\text{K} - \text{H}]^+$ species in positive mode and $[\text{M} - 2\text{H} + \text{Na}]^-$ and $[\text{M} - 2\text{H} + \text{K}]^-$ species in negative mode. Because these ions were not

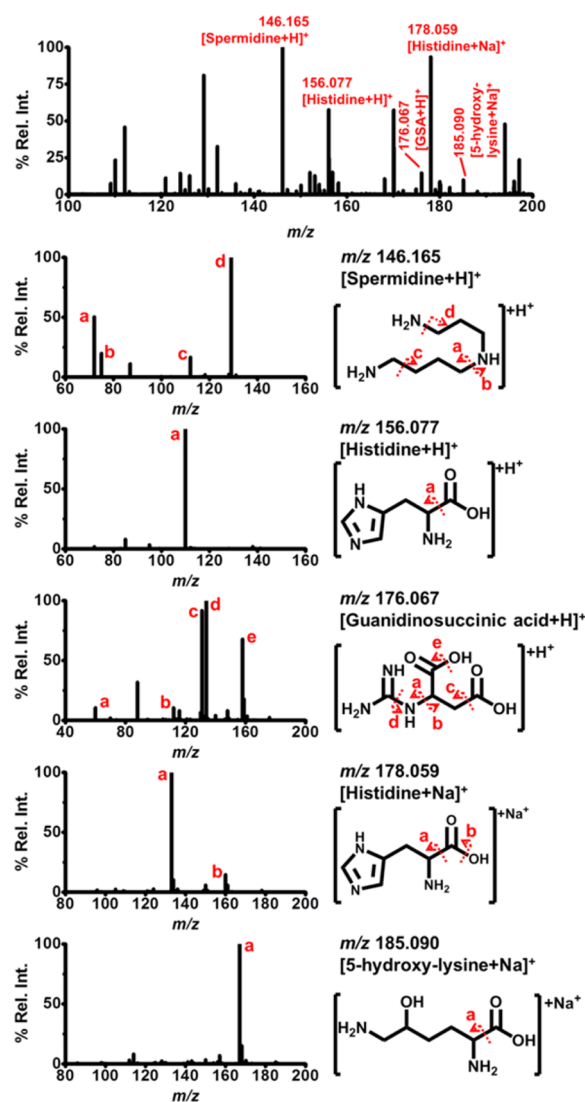


Figure 1. Positive ion mode NAPA-LDI-MS spectrum (top) and MS/MS spectra for several ions obtained from a mixture of 11 standards. Proposed fragment identities are denoted by letters in the spectra and on the structure.

identified until after acquisition, these masses were not considered for data-dependent MS/MS acquisition and thus no MS/MS spectra were collected. The reason for the comparatively high abundance of these ionic species relative to what is typically observed in MALDI or ESI is not immediately clear. However, this may be a result of the relatively high abundance of sodium cations present as counterions in many of the sample mixtures.

For 244/618 compounds, precursor ions were not detected in MS spectra under the selected set of conditions. Depending upon the compound, the lack of precursor ions can be explained by one or more factors. Some MS/MS compounds (e.g., phenylacetaldehyde) are expected to exhibit inherent low ionization efficiency due to a lack of readily ionizable functional groups (carboxyl, phosphate, sulfate, amine, etc.). Additionally, the combination of metabolite standards into mixtures of up to 12 compounds (along with all counterions, where present) could lead to suppression of ionization for certain species. Several compounds (e.g., benzaldehyde) are volatile and are likely to be lost during the drying step of the standard mixture

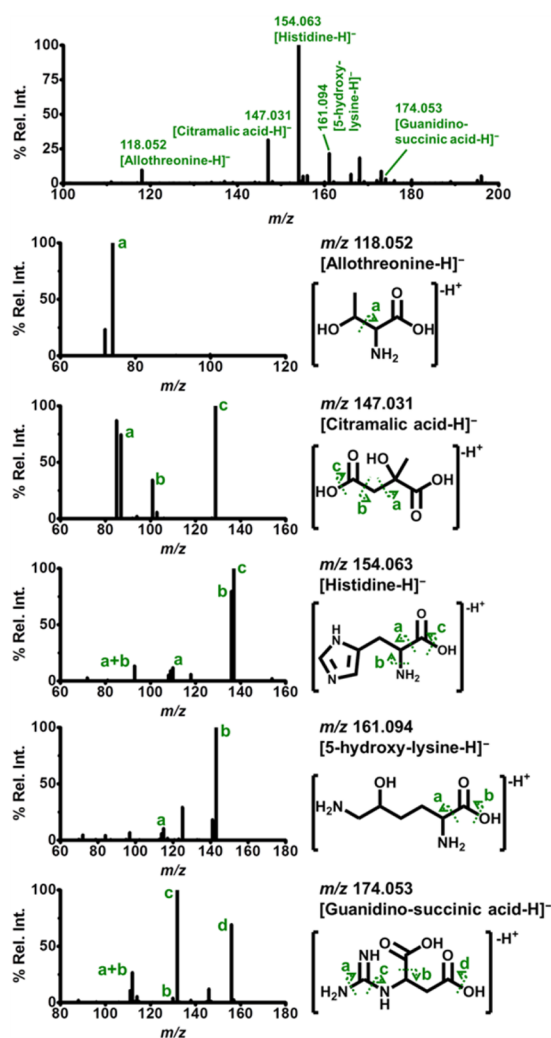


Figure 2. Negative ion mode NAPA-LDI-MS spectrum (top) and MS/MS spectra for several ions obtained from a mixture of 11 standards. Proposed fragment identities are denoted by letters in the spectra and on the structure.

Table 1. Summary of Metabolite Coverage in Positive Ion Mode

	MS and MS/MS	MS only
$[M + H]^+$	96	37
$[M + H - H_2O]^+$	35	34
$[M + Na]^+$	95	94
$[M + K]^+$	25	31
$[M + 2Na - H]^+$		141
$[M + 2K - H]^+$		31
total spectra	251	368
compounds covered	164	134

preparation or under the vacuum of the mass spectrometer source prior to analysis.

Compounds that are particularly labile are susceptible to fragmentation at elevated fluences and may not be detected in the ionic forms investigated (further discussion below). Finally, a total of 50 of the analyzed compounds have neutral masses outside the acquisition window of the performed experiments (m/z 100–1000; made necessary by an instrumental loss of sensitivity when expanding the scan range below m/z 100), although 7 of these compounds were detected as $[M + Na]^+$,

Table 2. Summary of Metabolite Coverage in Negative Ion Mode

	MS and MS/MS	MS only
$[M - H]^-$	221	39
$[M - H - H_2O]^-$	29	24
$[M - 2H + Na]^-$		20
$[M - 2H + K]^-$		8
total spectra	250	91
compounds covered	222	46

$[M + 2Na - H]^+$, or $[M + 2K - H]^+$ ions within the designated scan range.

Several of the factors resulting in the lack of precursor ions can be mitigated in additional experiments. For example, reducing the laser fluence can result in reduced propensity for fragmentation of labile compounds, whereas increasing the laser fluence can facilitate the ion production from compounds with inherently low ionization efficiency. Selective pooling of metabolites (e.g., by functionality) offers the potential to minimize suppression effects and would allow for the introduction of selected additives (acids, bases, metal cations, etc.) to improve ion yields, as often done in MALDI-MS.^{29–32}

Metabolic Pathway Coverage. To provide biological context for this large-scale screening, compound detection was examined as a function of metabolic pathway coverage. Detected compounds were compared to metabolic pathways as obtained from the Human Metabolome Database (HMDB; <http://www.hmdb.ca>, last accessed March 19, 2016).³³ This coverage is presented for several pathways in Figure 3. For most pathways, the collection of standards does not include all metabolite components. However, the kit contains 50% or greater of the metabolites for 23 of the 31 pathways presented in Figure 3. Within these 31 pathways, the average detection coverage (relative to compounds present in the MSMLS kit) was 63%. An average of 46% of pathway compounds yielded both MS detection and MS/MS spectra, while an average of 17% were detected in MS spectra only. A listing of the detected metabolites by pathway is provided in Spreadsheet S2 of the Supporting Information.

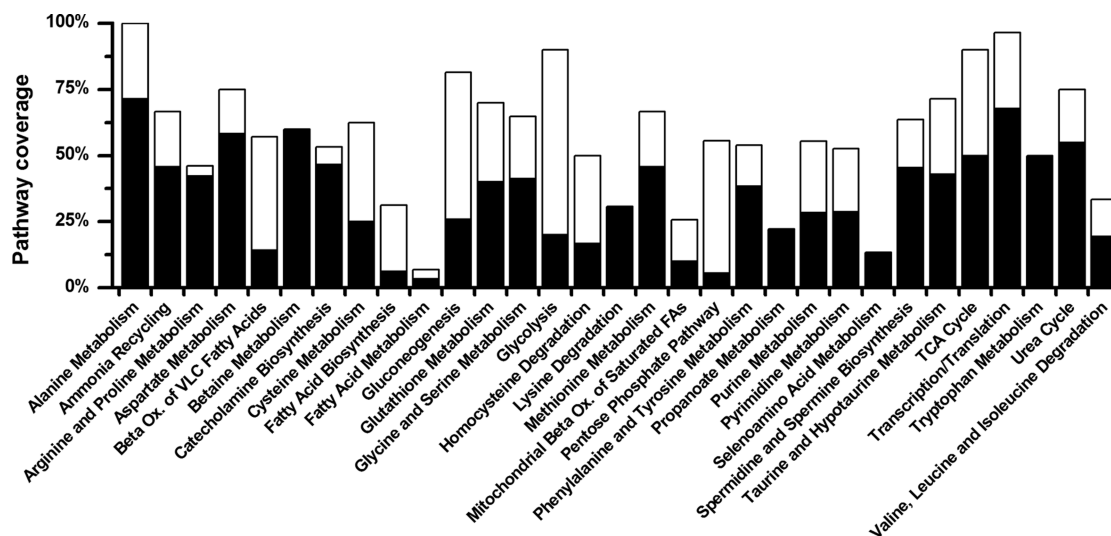


Figure 3. NAPA-LDI-MS coverage of metabolite standards for a single set of parameters (e.g., 40 mJ/cm² fluence) in several biological pathways. Black bars represent compounds for which standards were available and detected. White bars represent standards that were not detected under these circumstances.

Notably, of the compounds included in the collection of standards for metabolisms of alanine, arginine and proline, aspartate, betaine, phenylalanine and tyrosine, propanoate, selenoamino acid, and tryptophan and the biosynthesis of spermidine and spermine, and catecholamine, as well as protein transcription/translation, lysine degradation, and the urea cycle, the MS coverage was $\geq 70\%$. Comparatively poor coverage was obtained for fatty acid biosynthesis, homocysteine degradation, gluconeogenesis, glycolysis, and the pentose phosphate pathway.

Quantitative Response and Fluence Dependent Fragmentation. In addition to high sensitivity and reduced background, NAPA-LDI-MS had demonstrated a wide dynamic range for quantitation.^{18,21} Here, acetylcholine and cAMP were used in positive and negative mode, respectively, to evaluate the quantitation capabilities of the newer DUV-PL-produced NAPA for metabolite analysis (Figure 4). Both compounds offered a dynamic range of approximately 4 orders of magnitude before signal saturation above deposited amounts of $\sim 10^{-9}$ mol.

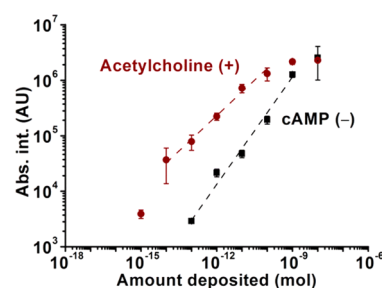


Figure 4. Metabolite NAPA-LDI-MS ion intensities as a function of deposited amount. Presented abundances of acetylcholine and cAMP are the intensities of $[M]^+$ and $[M - H]^-$, respectively. Linear regression lines span 4 orders of magnitude for each standard with R^2 values of >0.98 .

A unique feature of NAPA-LDI is the ability to control the internal energy deposited into the produced ions. At low

fluences predominantly intact molecular or pseudomolecular ions are formed, whereas at elevated fluences structure specific fragmentation takes place.³⁴ To demonstrate this feature, spectra were obtained from cAMP and acetylcholine standards at a range of fluences. The signal for the intact ions ($[\text{cAMP} - \text{H}]^-$ and $[\text{acetylcholine}]^+$) increased from the threshold for ion generation at $\sim 12 \text{ mJ/cm}^2$ to a maximum at $60\text{--}100 \text{ mJ/cm}^2$ before declining at even higher fluences. At 12 mJ/cm^2 , the intact $[\text{cAMP} - \text{H}]^-$ ion was observed with no detectable fragmentation, whereas at 40 mJ/cm^2 and above $[\text{adenine} - \text{H}]^-$ and $[\text{adenine} - \text{H} - \text{NH}_3]^-$ fragment peaks were observed and increased with increasing fluence. Similarly, abundance of the $[\text{acetylcholine}]^+$ signal was found to increase with increasing fluence to 60 mJ/cm^2 with fragments being observed at higher fluences. A comparison of cAMP spectra at low (40 mJ/cm^2) and high (400 mJ/cm^2) fluence is presented in Figure 5, and spectra of cAMP and acetylcholine at additional fluences

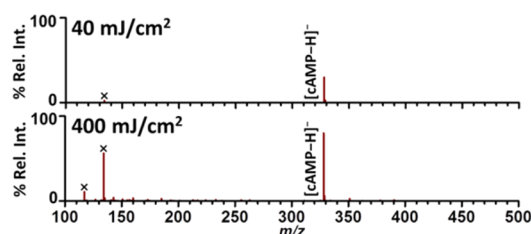


Figure 5. Mass spectra of 3',5'-cyclic adenosine monophosphate (cAMP) obtained by NAPA-LDI-MS at two laser fluences. Spectra are normalized to an absolute intensity of 1.2×10^6 au. Fragment ions $[\text{C}_5\text{H}_4\text{N}_5]^-$ and $[\text{C}_5\text{HN}_4]^-$ of cAMP are denoted by (X).

are shown in Figure S1 of the Supporting Information. As a compromise between increasing ion abundance and minimizing fragmentation, all acquisitions for the collection of standards were performed at a fluence of $\sim 40 \text{ mJ/cm}^2$.

Although structure specific fragmentation at high fluences can be detrimental for detection of intact analytes, it can be used to generate tandem MS-like ions for further structural analysis. A comparison of CID fragmentation spectra for $[\text{adenine} - \text{H}]^-$ ions generated by structure specific fragmentation and ion trap CID (Figure S2 in the Supporting Information) shows a high degree of similarity for the two methods of fragmentation, suggesting that NAPA-LDI selective fragmentation can provide an additional layer of structural analysis on instrumental platforms without MSⁿ capability.

Targeted Amino Acid Analysis. To evaluate the potential for improved metabolite coverage by targeted analysis of compounds, standards of the 20 common amino acids were analyzed individually. Spectra obtained for each amino acid in positive and negative modes are presented in Figures S3 and S4 in the Supporting Information, respectively. Amino acid-derived peaks were detected for 20/20 compounds in positive mode and 19/20 in negative mode. By comparison, analysis of these amino acids in the context of the large-scale screening experiment yielded an overall coverage of 17/20 compounds, with 14/20 detected in negative mode and 13/20 detected in positive mode. With the exception of cysteine, amino acid-derived peaks were detected as the base peak in both polarities in targeted experiments. Positive mode analysis yielded predominantly $[\text{M} + \text{H}]^+$, $[\text{M} + \text{Na}]^+$, and $[\text{M} + 2\text{Na} - \text{H}]^+$ ions, whereas negative mode analysis yielded predominantly $[\text{M} - \text{H}]^-$ ions along with deprotonated sodium adducts of the dimers ($[\text{2M} - 2\text{H} + \text{Na}]^-$) of several amino acids. Because

laser fluence was not individually optimized, fragment ions were observed for several amino acids. Tables of amino acid-derived signals are provided in Tables S1 and S2 in the Supporting Information.

Serum Extraction and Analysis. As a demonstration of the utility of NAPA-LDI-MS for metabolite profiling of biological samples, human serum extracts were analyzed. Full experimental details are available in the Supporting Information; briefly, the proteins were precipitated from serum aliquots, a two-phase extraction was performed to isolate polar and nonpolar metabolites, and the isolates were separately spotted and analyzed by NAPA-LDI-MS. A segment of a sample spectrum obtained from a serum extract is presented in Figure 6, and a list of the identified metabolites is provided in

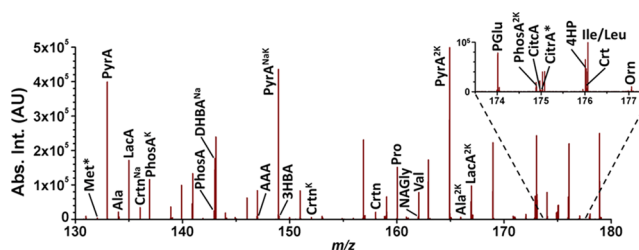


Figure 6. Segment of averaged positive ion mode spectrum obtained from NAPA-LDI-MS of aqueous serum extract with assigned metabolite peaks. Inset: expanded region from m/z 173.5–177.5. X*, X^{Na}, X^K, and X^{NaK} denote the $[\text{M} + \text{H} - \text{H}_2\text{O}]^+$, $[\text{M} + \text{Na}]^+$, $[\text{M} + \text{K}]^+$, and $[\text{M} + \text{Na} + \text{K} - \text{H}]^+$ species, respectively. All other species are detected as $[\text{M} + 2\text{Na} - \text{H}]^+$. Mass errors for all assigned species are $< 1 \text{ mDa}$. Met, methionine; PyrA, pyruvic acid; Ala, alanine; Laca, lactic acid; Crtn, creatinine; PhosA, phosphoric acid; DHBA, 3,4-dihydroxybutyric acid; AAA, acetoacetic acid; 3HBA, 3-hydroxybutanoic acid; Pro, proline; NAGly, N-acetylglycine; Val, valine; PGLu, pyroglutamic acid; CitcA, citraconic acid; CitcA*, citric acid; 4HP, trans-4-hydroxyproline; Ile/Leu, isoleucine/leucine; Crt, creatine; Orn, ornithine.

Tables S3–S6. Deisotoped spectral features were assigned to a total of 108 small metabolites and lipids by accurate mass search against the HMDB database, and in some cases by internal standards (glucose, arginine, phenylalanine, and proline). The tentatively assigned peaks belonged to glucose, cholesterol, amino acids, small organic acids, phospholipids, and fatty acids. Glucose, with a serum concentration of 5.2 mM according to the certificate, dominated the spectrum. Nonetheless, many lower-abundance metabolites were detected and spiking of serum samples prior to extraction was found to yield a quantitative response for both the highly abundant glucose and some much lower-abundance amino acids arginine, phenylalanine, and proline for up to 10 times their reported native concentrations³⁵ even without the addition of internal standards (see Figure S5). Improved metabolite coverage should be possible by introducing additional sample preparation steps, e.g., to remove carbohydrates or enrich for targeted analyte classes. The rapid analysis afforded by NAPA-LDI-MS allows for the integration of such steps without compromising the overall experimental throughput.

CONCLUSIONS

From large-scale, untargeted metabolite standard screening experiments, we have demonstrated the suitability of NAPA-LDI-MS for the detection and tandem MS analysis of a wide range of small molecule metabolites, with detection of 374

metabolites in at least one ionic form and significant coverage of several important metabolic pathways. The untargeted strategy employed for these experiments provided rapid screening of a vast array of metabolites, at the expense of individual optimization. We have also shown that greater coverage can be achieved by targeted analysis of individual metabolites or metabolite classes, such as amino acids. A number of additional factors remain open for exploration to expand molecular coverage, including variation of laser fluence, individual analysis or selective pooling of metabolites, and introduction of additives into sample solutions. Furthermore, improved tandem MS coverage should be possible by adjustment of fragmentation parameters such as collision energy and activation time. Finally, experiments are underway investigating functionalization of NAPA surfaces to enhance ionization of metabolites, either globally or for specific chemical classes. Nonetheless, the wide coverage obtained from untargeted screening experiments indicates significant versatility for the platform, essential to addressing the chemical diversity of metabolites, with focused analysis of specific compounds or compound classes expanding the utility even further.

The wide dynamic range exhibited for NAPA-LDI-MS, with ion signal proportional to loading amounts for over 4 orders of magnitude for sample metabolites, offers the potential for quantitation of metabolites over a significant concentration range. Finally, the tunable, fluence-dependent selective fragmentation, possible on NAPA platforms, was shown to produce tandem MS-like ions that allow for deeper structural analysis of NAPA-generated ions, facilitating identification of unknown metabolites or discrimination of isomers.

■ ASSOCIATED CONTENT

■ Supporting Information

The Supporting Information is available free of charge on the ACS Publications website at DOI: 10.1021/acs.analchem.6b01186.

Description of the serum extraction and analysis; representative NAPA-LDI mass spectra and fragmentation patterns as a function laser fluence, and amino acid spectra; ion intensities from spiked serum samples; tables of identified serum metabolites; tables of detected amino acid peaks (PDF)

Spreadsheet of detected metabolite ions (XLSX)

Spreadsheet of metabolic pathway coverage (XLSX)

■ AUTHOR INFORMATION

Corresponding Author

*E-mail: vertes@gwu.edu. Phone: +1 202-994-2717. Fax: +1 202-994-5873.

Notes

The authors declare no competing financial interest.

■ ACKNOWLEDGMENTS

Research was sponsored by the U.S. Army Research Office and the Defense Advanced Research Projects Agency and was accomplished under Cooperative Agreement Number W911NF-14-2-0020. The views and conclusions contained in this document are those of the authors and should not be interpreted as representing the official policies, either expressed or implied, of the Army Research Office, DARPA, or the U.S. Government. Application of the developed methods to complex

samples was supported by the Division of Chemical Sciences, Geosciences, and Biosciences, Office of Basic Energy Sciences of the U.S. Department of Energy through Grant DE-FG02-01ER15129.

■ REFERENCES

- (1) International Human Genome Sequencing Consortium; Lander, E. S.; Linton, L. M.; Birren, B.; Nusbaum, C.; Zody, M. C.; Baldwin, J.; Devon, K.; Dewar, K.; Doyle, M.; FitzHugh, W.; Funke, R.; Gage, D.; Harris, K.; Heaford, A.; Howland, J.; Kann, L.; LeHoczky, J.; LeVine, R.; McEwan, P.; McKernan, K.; Meldrum, J.; Mesirov, J. P.; Miranda, C.; Morris, W.; Naylor, J.; Raymond, C.; Rosetti, M.; Santos, R.; Sheridan, A.; Sougnez, C.; Stange-Thomann, N.; Stojanovic, N.; Subramanian, A.; Wyman, D.; Rogers, J.; Sulston, J.; Ainscough, R.; Beck, S.; Bentley, D.; Burton, J.; Clee, C.; Carter, N.; Coulson, A.; Deadman, R.; Deloukas, P.; Dunham, A.; Dunham, I.; Durbin, R.; French, L.; Grafham, D.; Gregory, C.; Hubbard, T.; Humphray, S.; Hunt, A.; Jones, M.; Lloyd, C.; McMurray, A.; Matthews, L.; Mercer, S.; Milne, S.; Mullikin, J. C.; Mungall, A.; Plumb, R.; Ross, M.; Shownkeen, R.; Sims, S.; Waterston, R. H.; Wilson, R. K.; Hillier, L. W.; McPherson, J. D.; Marra, M. A.; Mardis, E. R.; Fulton, L. A.; Chinwalla, A. T.; Pepin, K. H.; Gish, W. R.; Chissole, S. L.; Wendl, M. C.; Delehaunty, K. D.; Miner, T. L.; Delehaunty, A.; Kramer, J. B.; Cook, L. L.; Fulton, R. S.; Johnson, D. L.; Minx, P. J.; Clifton, S. W.; Hawkins, T.; Branscomb, E.; Predki, P.; Richardson, P.; Wenning, S.; Slezak, T.; Doggett, N.; Cheng, J. F.; Olsen, A.; Lucas, S.; Elkin, C.; Uberbacher, E.; Frazier, M.; Gibbs, R. A.; Muzny, D. M.; Scherer, S. E.; Bouck, J. B.; Sodergren, E. J.; Worley, K. C.; Rives, C. M.; Gorrell, J. H.; Metzker, M. L.; Naylor, S. L.; Kucherlapati, R. S.; Nelson, D. L.; Weinstock, G. M.; Sakaki, Y.; Fujiyama, A.; Hattori, M.; Yada, T.; Toyoda, A.; Itoh, T.; Kawagoe, C.; Watanabe, H.; Totoki, Y.; Taylor, T.; Weissbach, J.; Heilig, R.; Saurin, W.; Artiguenave, F.; Brottier, P.; Bruls, T.; Pelletier, E.; Robert, C.; Wincker, P.; Rosenthal, A.; Platzer, M.; Nyakatura, G.; Taudien, S.; Rump, A.; Yang, H. M.; Yu, J.; Wang, J.; Huang, G. Y.; Gu, J.; Hood, L.; Rowen, L.; Madan, A.; Qin, S. Z.; Davis, R. W.; Federspiel, N. A.; Abola, A. P.; Proctor, M. J.; Myers, R. M.; Schmutz, J.; Dickson, M.; Grimwood, J.; Cox, D. R.; Olson, M. V.; Kaul, R.; Shimizu, N.; Kawasaki, K.; Minoshima, S.; Evans, G. A.; Athanasiou, M.; Schultz, R.; Roe, B. A.; Chen, F.; Pan, H. Q.; Ramsay, J.; Lehrach, H.; Reinhardt, R.; McCombie, W. R.; de la Bastide, M.; Dedhia, N.; Blocker, H.; Hornischer, K.; Nordsiek, G.; Agarwala, R.; Aravind, L.; Bailey, J. A.; Bateman, A.; Batzoglu, S.; Birney, E.; Bork, P.; Brown, D. G.; Burge, C. B.; Cerutti, L.; Chen, H. C.; Church, D.; Clamp, M.; Copley, R. R.; Doerks, T.; Eddy, S. R.; Eichler, E. E.; Furey, T. S.; Galagan, J.; Gilbert, J. G. R.; Harmon, C.; Hayashizaki, Y.; Haussler, D.; Hermjakob, H.; Hokamp, K.; Jang, W. H.; Johnson, L. S.; Jones, T. A.; Kasif, S.; Kasprzyk, A.; Kennedy, S.; Kent, W. J.; Kitts, P.; Koonin, E. V.; Korf, I.; Kulp, D.; Lancet, D.; Lowe, T. M.; McLysaght, A.; Mikkelsen, T.; Moran, J. V.; Mulder, N.; Pollara, V. J.; Ponting, C. P.; Schuler, G.; Schultz, J. R.; Slater, G.; Smit, A. F. A.; Stupka, E.; Szustakowki, J.; Thierry-Mieg, D.; Thierry-Mieg, J.; Wagner, L.; Wallis, J.; Wheeler, R.; Williams, A.; Wolf, Y. I.; Wolfe, K. H.; Yang, S. P.; Yeh, R. F.; Collins, F.; Guyer, M. S.; Peterson, J.; Felsenfeld, A.; Wetterstrand, K. A.; Patrinos, A.; Morgan, M. J. *Nature* **2001**, *409*, 860–921.
- (2) Nagalakshmi, U.; Wang, Z.; Waern, K.; Shou, C.; Raha, D.; Gerstein, M.; Snyder, M. *Science* **2008**, *320*, 1344–1349.
- (3) Hebert, A. S.; Richards, A. L.; Bailey, D. J.; Ulbrich, A.; Coughlin, E. E.; Westphall, M. S.; Coon, J. J. *Mol. Cell. Proteomics* **2014**, *13*, 339–347.
- (4) Patti, G. J.; Yanes, O.; Siuzdak, G. *Nat. Rev. Mol. Cell Biol.* **2012**, *13*, 263–269.
- (5) Gika, H. G.; Theodoridis, G. A.; Plumb, R. S.; Wilson, I. D. J. *Pharm. Biomed. Anal.* **2014**, *87*, 12–25.
- (6) Wei, J.; Buriak, J. M.; Siuzdak, G. *Nature* **1999**, *399*, 243–246.
- (7) Chen, Y.; Vertes, A. *Anal. Chem.* **2006**, *78*, 5835–5844.

(8) Northen, T. R.; Yanes, O.; Northen, M. T.; Marrinucci, D.; Uritboonthai, W.; Apon, J.; Golledge, S. L.; Nordstrom, A.; Siuzdak, G. *Nature* **2007**, *449*, 1033–U3.

(9) Go, E. P.; Apon, J. V.; Luo, G. H.; Saghatelian, A.; Daniels, R. H.; Sahi, V.; Dubrow, R.; Cravatt, B. F.; Vertes, A.; Siuzdak, G. *Anal. Chem.* **2005**, *77*, 1641–1646.

(10) Piret, G.; Drobecq, H.; Coffinier, Y.; Melnyk, O.; Boukherroub, R. *Langmuir* **2010**, *26*, 1354–1361.

(11) Tanaka, K.; Waki, H.; Ido, Y.; Akita, S.; Yoshida, Y.; Yoshida, T.; Matsuo, T. *Rapid Commun. Mass Spectrom.* **1988**, *2*, 151–153.

(12) McLean, J. A.; Stumpo, K. A.; Russell, D. H. *J. Am. Chem. Soc.* **2005**, *127*, 5304–5305.

(13) Wen, X.; Dagan, S.; Wysocki, V. H. *Anal. Chem.* **2007**, *79*, 434–444.

(14) Chiang, C.-K.; Chen, W.-T.; Chang, H.-T. *Chem. Soc. Rev.* **2011**, *40*, 1269–1281.

(15) Walker, B. N.; Stolee, J. A.; Pickel, D. L.; Retterer, S. T.; Vertes, A. *J. Phys. Chem. C* **2010**, *114*, 4835–4840.

(16) Walker, B. N.; Stolee, J. A.; Vertes, A. *Anal. Chem.* **2012**, *84*, 7756–7762.

(17) Stolee, J. A.; Walker, B. N.; Zorba, V.; Russo, R. E.; Vertes, A. *Phys. Chem. Chem. Phys.* **2012**, *14*, 8453–8471.

(18) Walker, B. N.; Antonakos, C.; Retterer, S. T.; Vertes, A. *Angew. Chem., Int. Ed.* **2013**, *52*, 3650–3653.

(19) Karas, M.; Hillenkamp, F. *Anal. Chem.* **1988**, *60*, 2299–2301.

(20) Zenobi, R.; Knochenmuss, R. *Mass Spectrom. Rev.* **1998**, *17*, 337–366.

(21) Morris, N. J.; Anderson, H.; Thibeault, B.; Vertes, A.; Powell, M. J.; Razunguzwa, T. T. *RSC Adv.* **2015**, *5*, 72051–72057.

(22) Anderson, H.; Powell, M. J.; Morris, N. J.; Razunguzwa, T. T. In *Proceedings of the 63rd ASMS Conference on Mass Spectrometry and Allied Topics*, St. Louis, MO, June 3, 2015; p 1821.

(23) Stopka, S. A.; Rong, C.; Korte, A. R.; Yadavilli, S.; Nazarian, J.; Razunguzwa, T. T.; Morris, N. J.; Vertes, A. *Angew. Chem., Int. Ed.* **2016**, *55*, 4482–4486.

(24) Junot, C.; Fenaille, F.; Colsch, B.; Becher, F. *Mass Spectrom. Rev.* **2014**, *33*, 471–500.

(25) Xian, F.; Hendrickson, C. L.; Marshall, A. G. *Anal. Chem.* **2012**, *84*, 708–719.

(26) Baeten, W.; Claereboudt, J.; Vandenheuvel, H.; Claeys, M. *Biomed. Environ. Mass Spectrom.* **1989**, *18*, 727–732.

(27) Moberg, M.; Markides, K. E.; Bylund, D. J. *Mass Spectrom.* **2005**, *40*, 317–324.

(28) Stolee, J. A.; Walker, B. N.; Chen, Y.; Vertes, A. In *International Symposium on High Power Laser Ablation 2010*, Phipps, C. R., Ed.; 2010; Vol. 1278, pp 98–110.

(29) Kjellstrom, S.; Jensen, O. N. *Anal. Chem.* **2004**, *76*, 5109–5117.

(30) Cerruti, C. D.; Touboul, D.; Guerineau, V.; Petit, V. W.; Laprevote, O.; Brunelle, A. *Anal. Bioanal. Chem.* **2011**, *401*, 75–87.

(31) Sedo, O.; Sedlacek, I.; Zdrahal, Z. *Mass Spectrom. Rev.* **2011**, *30*, 417–434.

(32) Griffiths, R. L.; Bunch, J. *Rapid Commun. Mass Spectrom.* **2012**, *26*, 1557–1566.

(33) Wishart, D. S.; Jewison, T.; Guo, A. C.; Wilson, M.; Knox, C.; Liu, Y.; Djoumbou, Y.; Mandal, R.; Aziat, F.; Dong, E.; Bouatra, S.; Sinelnikov, I.; Arndt, D.; Xia, J.; Liu, P.; Yallou, F.; Bjorn Dahl, T.; Perez-Pineiro, R.; Eisner, R.; Allen, F.; Neveu, V.; Greiner, R.; Scalbert, A. *Nucleic Acids Res.* **2013**, *41*, D801–D807.

(34) Stolee, J. A.; Vertes, A. *Phys. Chem. Chem. Phys.* **2011**, *13*, 9140–9146.

(35) Psychogios, N.; Hau, D. D.; Peng, J.; Guo, A. C.; Mandal, R.; Bouatra, S.; Sinelnikov, I.; Krishnamurthy, R.; Eisner, R.; Gautam, B.; Young, N.; Xia, J. G.; Knox, C.; Dong, E.; Huang, P.; Hollander, Z.; Pedersen, T. L.; Smith, S. R.; Bamforth, F.; Greiner, R.; McManus, B.; Newman, J. W.; Goodfriend, T.; Wishart, D. S. *PLoS One* **2011**, *6*, e16957.

Supporting Information

Large-Scale Metabolite Analysis by Laser Desorption Ionization Mass Spectrometry from Silicon Nanopost Arrays

Andrew R. Korte[†], Sylwia A. Stopka[†], Nicholas Morris[‡], Trust Razunguzwa[‡], and Akos Vertes^{†*}

[†]Department of Chemistry, George Washington University, Washington, DC 20052, USA

[‡]Protea Biosciences, Inc., Morgantown, WV 26505, USA

*Corresponding Author

Email: vertes@gwu.edu (A. Vertes). Phone: +1 202-994-2717. Fax: +1 202-994-5873. Address: Department of Chemistry, The George Washington University, 800 22-nd Street, N.W., Washington, DC 20052, USA.

Table of Contents

Supplement for EXPERIMENTAL SECTION	S-3
Supplementary Figures	S-4 to S-8
Supplementary Tables	S-9 to S-18
REFERENCES	S-19

IN SEPARATE FILES:

Spreadsheet S1. All metabolite ions detected in NAPA-LDI-MS analysis of standard mixtures.

Spreadsheet S2. Detected metabolites within the metabolic pathways presented in Figure 3.

Supplement for EXPERIMENTAL SECTION

Serum extraction and analysis. Human Serum Type AB, Male (Cat. No. H4522 and Lot No. SLBN9196V) was purchased from Sigma-Aldrich (St. Louis, MO). Proteins were precipitated from 100 μL aliquots of the serum by the addition of 400 μL of $-20\text{ }^{\circ}\text{C}$ methanol. After methanol addition, the samples were vortexed briefly to mix, sonicated for 5 min, and incubated at $-20\text{ }^{\circ}\text{C}$ for 1 h. They were then centrifuged for 10 min at $14,000 \times g$ and $4\text{ }^{\circ}\text{C}$.

The supernatant was transferred to a fresh sample tube, and 400 μL of $-20\text{ }^{\circ}\text{C}$ chloroform and 100 μL of $4\text{ }^{\circ}\text{C}$ water were added to each sample, inducing separation into organic and aqueous phases. The samples were then briefly vortexed and centrifuged for 10 min at $14,000 \times g$ and $4\text{ }^{\circ}\text{C}$. The organic and aqueous phases from each sample were removed to separate sample tubes and dried in a vacuum centrifuge at $4\text{ }^{\circ}\text{C}$, then stored at $-80\text{ }^{\circ}\text{C}$ until use.

Aqueous extracts were reconstituted in 100 μL of water and 0.5 μL was spotted onto each nanopost array. Organic extracts were reconstituted in 10 μL of 1:1 acetone:water and 0.2 μL was spotted onto each nanopost array. All extract samples were analyzed using a fluence of $100\text{ mJ}/\text{cm}^2$, three laser shots per scan, and one scan per raster point. The full area of each array was sampled at a raster pitch of 100 μm . Spectra were acquired in the orbitrap analyzer using a resolving power setting of 30,000, and m/z ranges of 100-600 for aqueous extracts and 200-1000 for organic extracts.

For standard addition experiments in which serum samples were spiked with known concentrations of metabolites, standards of glucose or an amino acid mixture (arginine, phenylalanine, and proline) were prepared in water and diluted to a range of concentrations. Concentrations of the spike solutions were selected such that final serum concentrations of the metabolites were $\sim 1\times$ (unspiked), $\sim 1.5\times$, $\sim 2\times$, $\sim 3\times$, $\sim 5\times$, and $\sim 10\times$ the reported natural concentrations¹. Prior to protein precipitation, 10 μL of the standard solution was added to the raw serum and samples were processed as above.

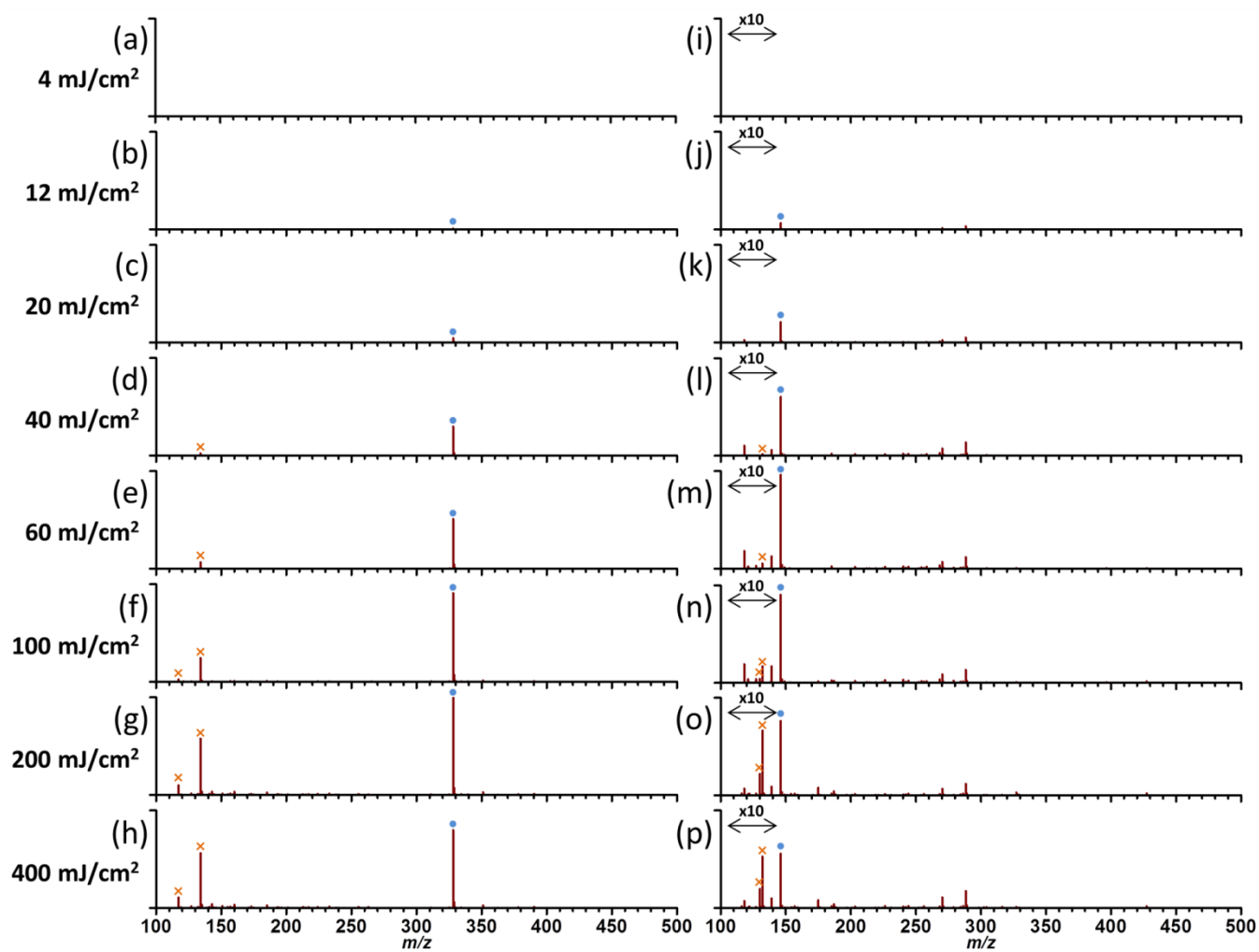


Figure S1. Mass spectra obtained from NAPA-LDI-MS of (a-h) 3',5'-cyclic adenosine monophosphate (cAMP) and (i-p) acetylcholine at a range of laser fluences. Intact metabolite ions ($[M]^+$ for acetylcholine and $[M-H]^-$ for cAMP) are denoted by (•), whereas (×) denotes fragment ions. cAMP and acetylcholine spectra are normalized to absolute intensities of 1.2×10^6 au and 2.0×10^6 au, respectively.

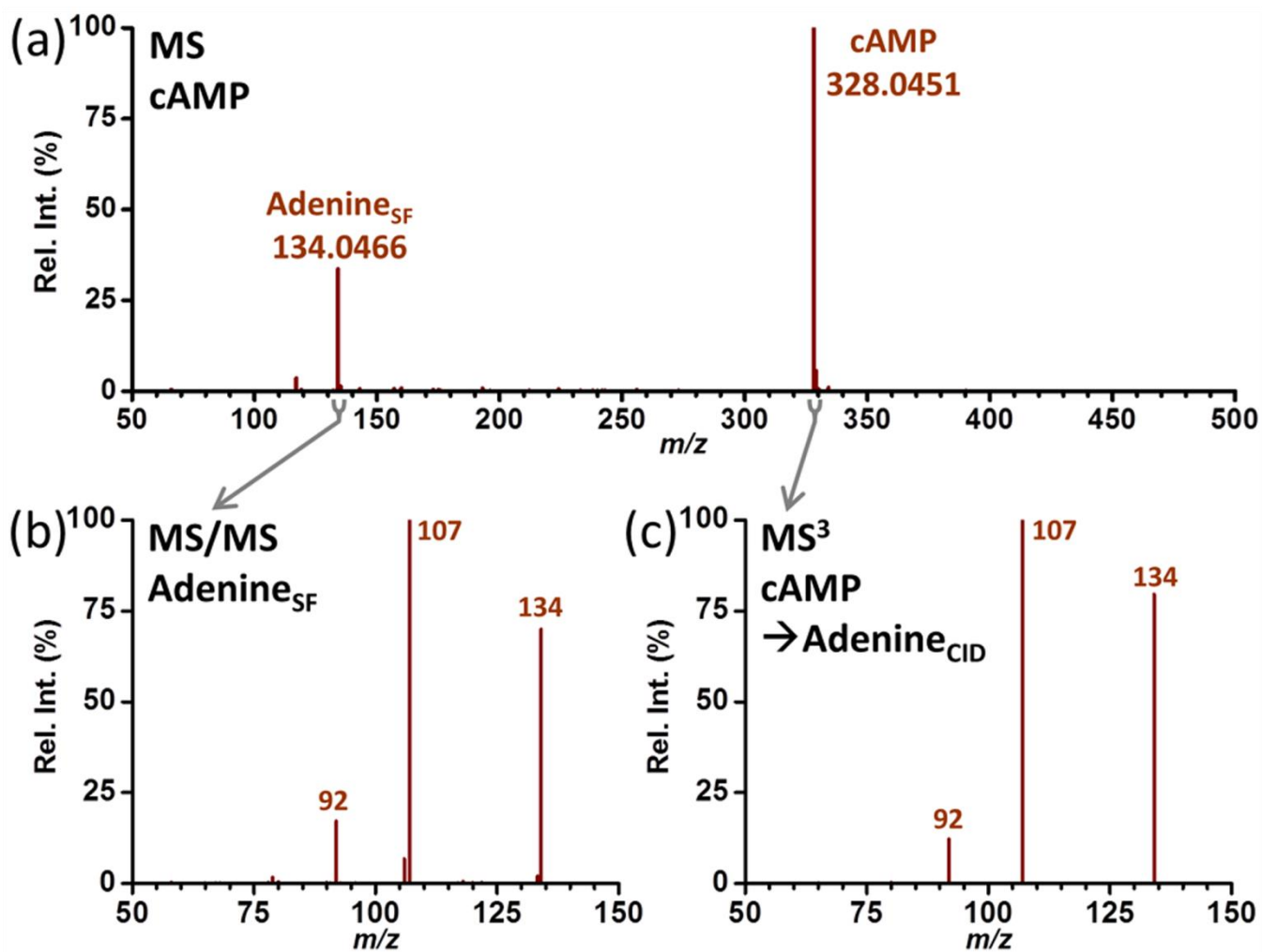


Figure S2. (a) MS spectrum of cAMP standard at 100 mJ/cm² fluence showing structure specific fragmentation (SF) to adenine ion. (b) MS/MS spectrum of adenine generated by structure specific fragmentation of cAMP. (c) MS³ spectrum of adenine generated by CID fragmentation of cAMP.

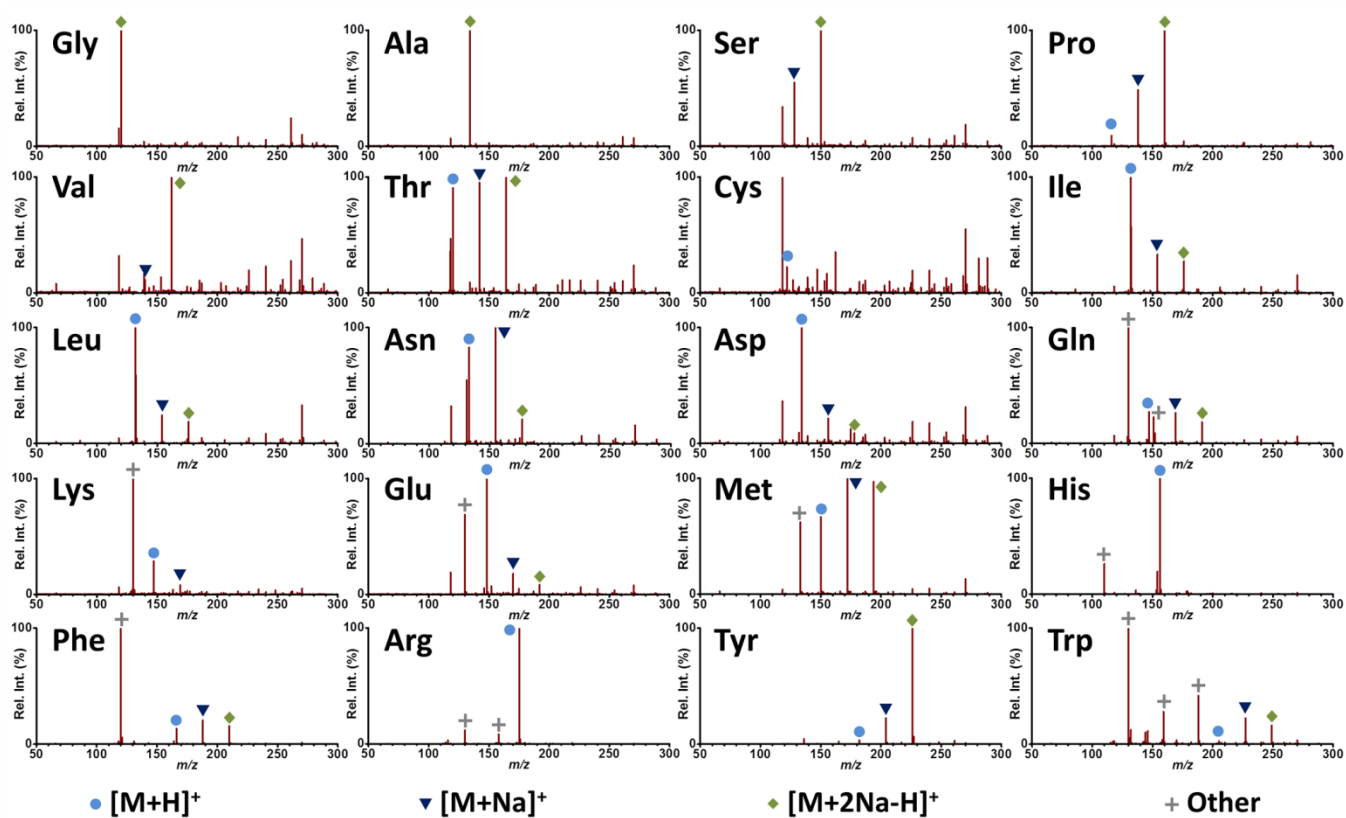


Figure S3. Positive ion mode NAPA-LDI-MS spectra of L-amino acid standards.

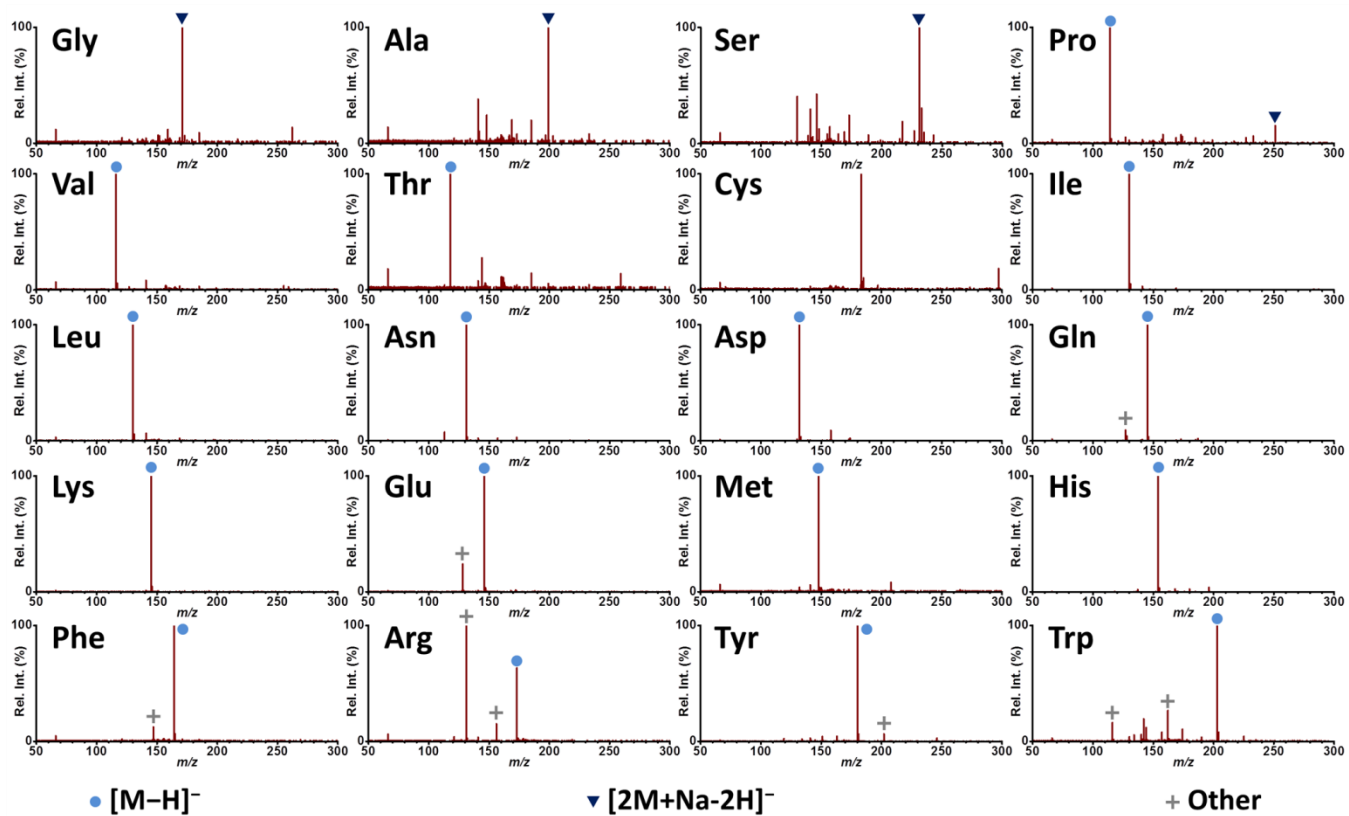


Figure S4. Negative ion mode NAPA-LDI-MS spectra of L-amino acids standards.

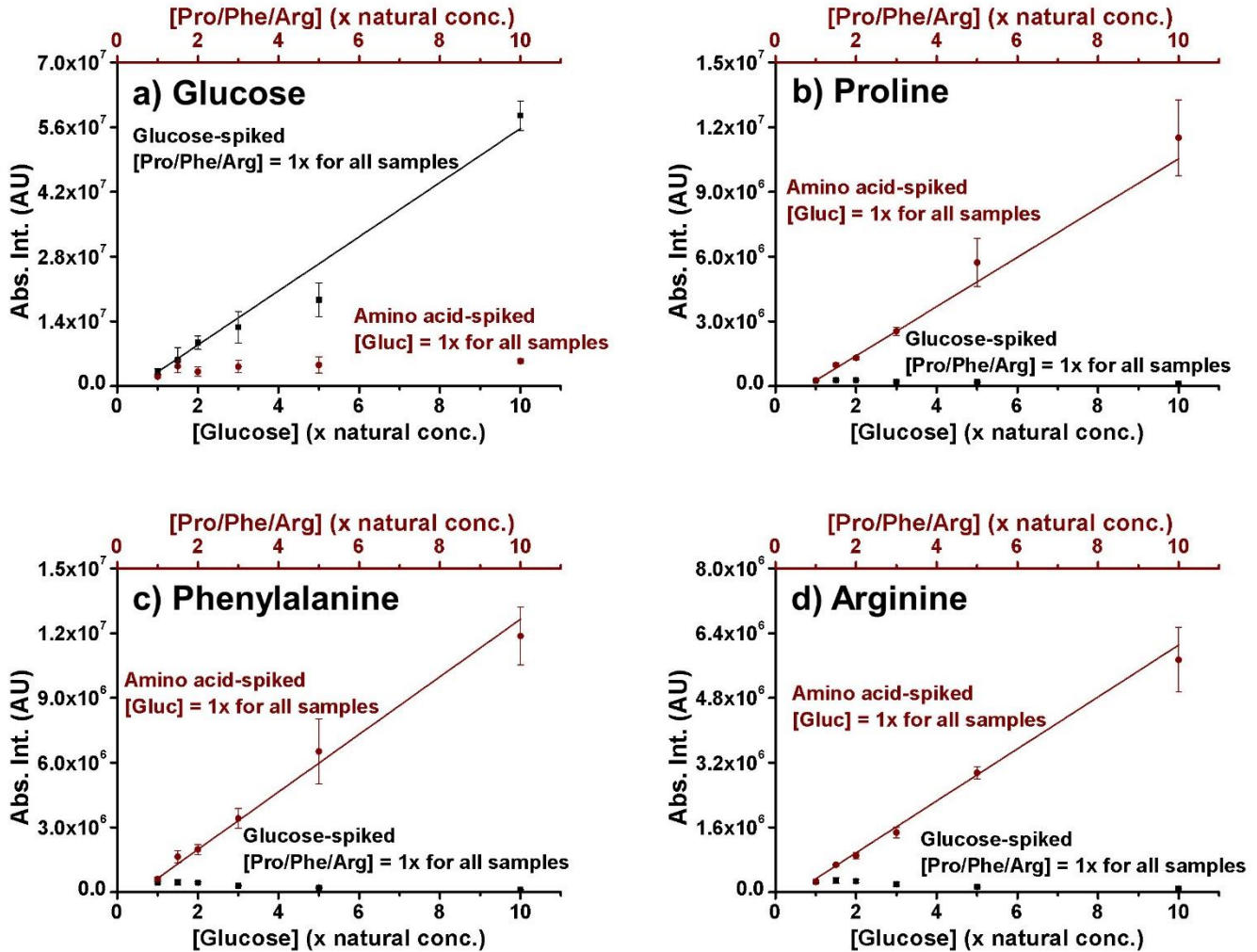


Figure S5. Summed absolute ion intensities for (a) glucose, (b) proline, (c) phenylalanine, and (d) arginine ions as a function of serum spike concentration. Glucose signal includes $[M+Na]^+$ and $[M+K]^+$ species and amino acid signals include $[M+2Na-H]^+$, $[M+Na+K-H]^+$, and $[M+2Na-H]^+$ species. Glucose-spiked standards were spiked with glucose in water, while amino acid-spiked standards were spiked with a mixture of proline, phenylalanine, and arginine in water. R^2 coefficients are 0.97 for glucose in glucose-spiked serum and >0.99 for the three amino acids in amino-acid spiked serum.

Table S1. Identified ions from positive ion mode analysis of individual L-amino acid standards

Amino acid	<i>m/z</i>	ID	Composition	Error (mDa)
Glycine	120.0032	[M+2Na-H] ⁺	C ₂ H ₄ O ₂ NNa ₂	0.1
Alanine	134.0192	[M+2Na-H] ⁺	C ₃ H ₆ O ₂ NNa ₂	0.3
Serine	128.0320	[M+Na] ⁺	C ₃ H ₇ O ₃ NNa	0.2
	150.0139	[M+2Na-H] ⁺	C ₃ H ₆ O ₃ NNa ₂	0.1
Proline	116.0707	[M+H] ⁺	C ₅ H ₁₀ O ₂ N	0.1
	138.0528	[M+Na] ⁺	C ₅ H ₉ O ₂ NNa	0.3
	160.0345	[M+2Na-H] ⁺	C ₅ H ₈ O ₂ NNa ₂	0.0
Valine	140.0685	[M+Na] ⁺	C ₅ H ₁₁ O ₂ NNa	0.3
	162.0506	[M+2Na-H] ⁺	C ₅ H ₁₀ O ₂ NNa ₂	0.5
Threonine	120.0656	[M+H] ⁺	C ₄ H ₁₀ O ₃ N	0.0
	142.0477	[M+Na] ⁺	C ₄ H ₉ O ₃ NNa	0.3
	164.0296	[M+2Na-H] ⁺	C ₄ H ₈ O ₃ NNa ₂	0.2
Cysteine	122.0272	[M+H] ⁺	C ₃ H ₈ O ₂ NS	0.2
Isoleucine	132.1023	[M+H] ⁺	C ₆ H ₁₄ O ₂ N	0.4
	154.0842	[M+Na] ⁺	C ₆ H ₁₃ O ₂ NNa	0.3
	176.0662	[M+2Na-H] ⁺	C ₆ H ₁₂ O ₂ NNa ₂	0.4
Leucine	132.1023	[M+H] ⁺	C ₆ H ₁₄ O ₂ N	0.4
	154.0842	[M+Na] ⁺	C ₆ H ₁₃ O ₂ NNa	0.4
	176.0662	[M+2Na-H] ⁺	C ₆ H ₁₂ O ₂ NNa ₂	0.4
Asparagine	133.0612	[M+H] ⁺	C ₄ H ₉ O ₃ N ₂	0.5
	155.0431	[M+Na] ⁺	C ₄ H ₈ O ₃ N ₂ Na	0.3
	177.0252	[M+2Na-H] ⁺	C ₄ H ₇ O ₃ N ₂ Na ₂	0.5
Aspartic acid	134.0452	[M+H] ⁺	C ₄ H ₈ O ₄ N	0.4
	156.0271	[M+Na] ⁺	C ₄ H ₇ O ₄ NNa	0.4
	178.0091	[M+2Na-H] ⁺	C ₄ H ₆ O ₄ NNa ₂	0.4
Glutamine	130.0503	[M+H-NH ₃] ⁺	C ₅ H ₈ O ₃ N	0.4
	147.0768	[M+H] ⁺	C ₅ H ₁₁ O ₃ N ₂	0.4
	151.0482	[M+Na-H ₂ O] ⁺	C ₅ H ₈ O ₂ N ₂ Na	0.4
	169.0589	[M+Na] ⁺	C ₅ H ₁₀ O ₃ N ₂ Na	0.5
	191.0408	[M+2Na-H] ⁺	C ₅ H ₉ O ₃ N ₂ Na ₂	0.5
Lysine	130.0866	[M+H-NH ₃] ⁺	C ₆ H ₁₂ O ₂ N	0.4
	147.1132	[M+H] ⁺	C ₆ H ₁₅ O ₂ N ₂	0.4
	169.0953	[M+Na] ⁺	C ₆ H ₁₄ O ₂ N ₂ Na	0.6
Glutamic acid	130.0503	[M+H-H ₂ O] ⁺	C ₅ H ₈ O ₃ N	0.4
	148.0608	[M+H] ⁺	C ₅ H ₁₀ O ₄ N	0.3
	170.0428	[M+Na] ⁺	C ₅ H ₉ O ₄ NNa	0.5
	192.0249	[M+2Na-H] ⁺	C ₅ H ₈ O ₄ NNa ₂	0.6

Methionine	133.0323	$[M+H-NH_3]^+$	$C_5H_9O_2S$	0.5
	150.0587	$[M+H]^+$	$C_5H_{12}O_2NS$	0.4
	172.0407	$[M+Na]^+$	$C_5H_{11}O_2NNaS$	0.4
	194.0227	$[M+2Na-H]^+$	$C_5H_{10}O_2NNa_2S$	0.5
Histidine	110.0714	$[M+H-H_2CO_2]^+$	$C_5H_8N_3$	0.1
	156.0770	$[M+H]^+$	$C_6H_{10}O_2N_3$	0.2
Phenylalanine	120.0809	$[M+H-H_2CO_2]^+$	$C_8H_{10}N$	0.2
	166.0866	$[M+H]^+$	$C_9H_{12}O_2N$	0.4
	188.0687	$[M+Na]^+$	$C_9H_{11}O_2NNa$	0.5
	210.0506	$[M+2Na-H]^+$	$C_9H_{10}O_2NNa_2$	0.5
Arginine	130.0978	$[M+H-CH_3NO]^+$	$C_5H_{12}ON_3$	0.3
	158.0927	$[M+H-NH_3]^+$	$C_6H_{12}O_2N_3$	0.3
	175.1193	$[M+H]^+$	$C_6H_{15}O_2N_4$	0.4
Tyrosine	182.0817	$[M+H]^+$	$C_9H_{12}O_3N$	0.6
	204.0635	$[M+Na]^+$	$C_9H_{11}O_3NNa$	0.4
	226.0455	$[M+2Na-H]^+$	$C_9H_{10}O_3NNa_2$	0.4
Tryptophan	130.0654	$[M+H-C_2H_5NO_2]^+$	C_9H_8N	0.3
	159.0919	$[M+H-CH_2O_2]^+$	$C_{10}H_{11}N_2$	0.2
	188.0710	$[M+H-NH_3]^+$	$C_{11}H_{10}O_2N$	0.4
	205.0976	$[M+H]^+$	$C_{11}H_{13}O_2N_2$	0.4
	227.0795	$[M+Na]^+$	$C_{11}H_{12}O_2N_2Na$	0.4
	249.0615	$[M+2Na-H]^+$	$C_{11}H_{11}O_2N_2Na_2$	0.4

Table S2. Identified ions from negative ion mode analysis of individual L-amino acid standards

Amino acid	<i>m/z</i>	ID	Composition	Error (mDa)
Glycine	171.0386	[2M+Na-2H] ⁻	C ₄ H ₈ O ₄ N ₂ Na	-0.1
Alanine	199.0705	[2M+Na-2H] ⁻	C ₆ H ₁₂ O ₄ N ₂ Na	0.5
Serine	231.0613	[2M+Na-2H] ⁻	C ₆ H ₁₂ O ₆ N ₂ Na	1.4
Proline	114.0560	[M-H] ⁻	C ₅ H ₈ O ₂ N	-0.1
	251.1033	[2M+Na-2H] ⁻	C ₁₀ H ₁₆ O ₄ N ₂ Na	2.0
Valine	116.0714	[M-H] ⁻	C ₅ H ₁₀ O ₂ N	-0.3
Threonine	118.0507	[M-H] ⁻	C ₄ H ₈ O ₃ N	-0.2
Cysteine	-	-	-	-
Isoleucine	130.0871	[M-H] ⁻	C ₆ H ₁₂ O ₂ N	-0.2
Leucine	130.0871	[M-H] ⁻	C ₆ H ₁₂ O ₂ N	-0.2
Asparagine	131.0461	[M-H] ⁻	C ₄ H ₇ O ₃ N ₂	-0.1
Aspartic acid	132.0303	[M-H] ⁻	C ₄ H ₆ O ₄ N	0.1
Glutamine	127.0507	[M-H] ⁻	C ₅ H ₇ O ₂ N ₂	0.0
	145.0619	[M-H] ⁻	C ₅ H ₉ O ₃ N ₂	0.0
Lysine	145.0983	[M-H] ⁻	C ₆ H ₁₃ O ₂ N ₂	0.0
Glutamic acid	128.0351	[M-H] ⁻	C ₅ H ₆ O ₃ N	-0.2
	146.0460	[M-H] ⁻	C ₅ H ₈ O ₄ N	0.1
Methionine	148.0437	[M-H] ⁻	C ₅ H ₁₀ O ₂ NS	-0.1
Histidine	154.0625	[M-H] ⁻	C ₆ H ₈ O ₂ N ₃	0.3
Phenylalanine	147.0452	[M-H-NH ₃] ⁻	C ₉ H ₇ O ₂	0.0
	164.0714	[M-H] ⁻	C ₉ H ₁₀ O ₂ N	-0.3
Arginine	131.0819	[M-H-CH ₂ N ₂] ⁻	C ₅ H ₁₁ O ₂ N ₂	-0.3
	156.0776	[M-H-NH ₃] ⁻	C ₆ H ₁₀ O ₂ N ₃	0.5
	173.1050	[M-H] ⁻	C ₆ H ₁₃ O ₂ N ₄	0.0
Tyrosine	180.0663	[M-H] ⁻	C ₉ H ₁₀ O ₃ N	-0.3
	202.0482	[M-2H+Na] ⁻	C ₉ H ₉ O ₃ NNa	-0.3
Tryptophan	116.0512	[M-H-C ₃ H ₅ NO ₂] ⁻	C ₈ H ₆ N	0.6
	162.0560	[M-H-C ₂ H ₃ N] ⁻	C ₉ H ₈ O ₂ N	-0.1
	203.0828	[M-H] ⁻	C ₁₁ H ₁₁ O ₂ N ₂	0.2

Table S3. Tentatively assigned ionic species detected in positive ion mode NAPA-LDI-MS analysis of aqueous phase serum extracts.

<i>m/z</i>	Assignment	Ion	Error (mDa)
118.0858	Betaine	[M+H] ⁺	-0.5
120.9658	Phosphoric acid	[M+Na] ⁺	-0.3
122.9238	Formic acid	[M+2K-H] ⁺	-0.7
132.0474	Methionine	[M+H-H ₂ O] ⁺	-0.4
132.987	Pyruvic acid	[M+2Na-H] ⁺	-0.2
134.0186	Alanine	[M+2Na-H] ⁺	-0.2
135.0026	Lactic acid	[M+2Na-H] ⁺	-0.3
136.0478	Creatinine	[M+Na] ⁺	-0.3
136.9399	Phosphoric acid	[M+K] ⁺	-0.2
142.9477	Phosphoric acid	[M+2Na-H] ⁺	-0.4
143.0312	3,4-dihydroxybutyric acid	[M+Na] ⁺	-0.3
147.0026	Acetoacetic acid	[M+2Na-H] ⁺	-0.3
148.9608	Pyruvic acid	[M+Na+K-H] ⁺	-0.3
149.0181	3-hydroxybutanoic acid	[M+2Na-H] ⁺	-0.4
152.0217	Creatinine	[M+K] ⁺	-0.4
158.0296	Creatinine	[M+2Na-H] ⁺	-0.5
160.0341	Proline	[M+2Na-H] ⁺	-0.4
162.0134	N-Acetylglycine	[M+2Na-H] ⁺	-0.4
162.0497	Valine	[M+2Na-H] ⁺	-0.4
164.9347	Pyruvic acid	[M+2K-H] ⁺	-0.4
165.9664	Alanine	[M+2K-H] ⁺	-0.3
166.9505	Lactic acid	[M+2K-H] ⁺	-0.2
174.0134	Pyroglutamic acid	[M+2Na-H] ⁺	-0.4
174.8956	Phosphoric acid	[M+2K-H] ⁺	-0.3
174.9976	Citraconic acid	[M+2Na-H] ⁺	-0.2
175.024	Citric acid	[M+H-H ₂ O] ⁺	0.3
176.029	Trans-4-hydroxyproline	[M+2Na-H] ⁺	-0.4
176.0401	Creatine	[M+2Na-H] ⁺	-0.5
176.0654	Leucine/isoleucine	[M+2Na-H] ⁺	-0.4
177.0616	Ornithine	[M+2Na-H] ⁺	0.6
183.0026	Salicylic acid	[M+2Na-H] ⁺	-0.3
191.0399	Glutamine	[M+2Na-H] ⁺	-0.4
191.077	Lysine	[M+2Na-H] ⁺	0.3
191.982	Proline	[M+2K-H] ⁺	-0.4
193.9978	Valine	[M+2K-H] ⁺	-0.2
200.0404	Histidine	[M+2Na-H] ⁺	-0.2
203.0522	Hexose	[M+Na] ⁺	-0.4
205.9613	Pyroglutamic acid	[M+2K-H] ⁺	-0.3
207.9769	Trans-4-hydroxyproline	[M+2K-H] ⁺	-0.4

208.0133	Leucine/isoleucine	$[M+2K-H]^+$	-0.4
210.0497	Phenylalanine	$[M+2Na-H]^+$	-0.4
219.0261	Hexose	$[M+K]^+$	-0.5
219.0824	Arginine	$[M+2Na-H]^+$	-0.4
222.9878	Glutamine	$[M+2K-H]^+$	-0.4
226.0446	Tyrosine	$[M+2Na-H]^+$	-0.5
233.0866	N-alpha-acetyl-L-lysine	$[M+2Na-H]^+$	-0.7
241.9976	Phenylalanine	$[M+2K-H]^+$	-0.4
249.0606	Tryptophan	$[M+2Na-H]^+$	-0.4
251.0305	Arginine	$[M+2K-H]^+$	-0.2
265.0345	N-alpha-acetyl-L-lysine	$[M+2K-H]^+$	-0.6
273.1794	Myristic acid	$[M+2Na-H]^+$	-0.7
279.2285	Palmitic acid	$[M+Na]^+$	-1.0
299.1949	Palmitelaidic acid	$[M+2Na-H]^+$	-0.8
301.2109	Palmitic acid	$[M+2Na-H]^+$	-0.5
303.2291	Linoleic acid	$[M+Na]^+$	-0.4
305.245	Oleic acid	$[M+Na]^+$	-0.1
325.2107	Linoleic acid	$[M+2Na-H]^+$	-0.7
327.2264	Oleic acid	$[M+2Na-H]^+$	-0.7
329.2421	Stearic acid	$[M+2Na-H]^+$	-0.6
387.0912	Maltose	$[M+2Na-H]^+$	3.8

Table S4. Tentatively assigned ionic species detected in negative ion mode NAPA-LDI-MS analysis of aqueous phase serum extracts.

<i>m/z</i>	Assignment	Ion	Error (mDa)
121.0297	Benzoic acid	[M-H] ⁻	0.2
127.0515	Glutamine	[M-H-H ₂ O] ⁻	0.2
127.0879	Lysine	[M-H-H ₂ O] ⁻	0.2
128.0354	Pyroglutamic acid	[M-H] ⁻	0.1
130.0624	Creatine	[M-H] ⁻	0.2
130.0872	Leucine/isoleucine	[M-H] ⁻	-0.1
137.0243	Salicylic acid	[M-H] ⁻	-0.1
145.0617	Glutamine	[M-H] ⁻	-0.2
146.0611	Phenylalanine	[M-H-H ₂ O] ⁻	-0.0
150.0561	Acetaminophen	[M-H] ⁻	0.1
154.062	Histidine	[M-H] ⁻	-0.2
161.0457	Hexose	[M-H-H ₂ O] ⁻	0.2
162.0562	Tyrosine	[M-H-H ₂ O] ⁻	0.2
164.0715	Phenylalanine	[M-H] ⁻	-0.2
168.0426	Leucine/isoleucine	[M-2H+K] ⁻	-0.6
169.0982	N-alpha-acetyl-L-lysine	[M-H-H ₂ O] ⁻	-0.0
180.067	Tyrosine	[M-H] ⁻	0.4
185.0716	Tryptophan	[M-H-H ₂ O] ⁻	-0.4
189.0026	Uric acid	[M-2H+Na] ⁻	-0.4
202.0501	Tyrosine	[M-2H+Na] ⁻	1.5
203.0828	Tryptophan	[M-H] ⁻	0.2
209.0935	Capric acid	[M-2H+K] ⁻	-1.4
227.2022	Myristic acid	[M-H] ⁻	0.5
237.125	Dodecanoic acid	[M-2H+K] ⁻	-1.2
253.2176	Palmitelaidic acid	[M-H] ⁻	0.3
255.2334	Palmitic acid	[M-H] ⁻	0.5
269.2495	Heptadecanoic acid	[M-H] ⁻	0.9
279.2328	Linoleic acid	[M-H] ⁻	-0.2
281.2482	Oleic acid	[M-H] ⁻	-0.4
283.264	Stearic acid	[M-H] ⁻	-0.3

Table S5. Tentatively assigned ionic species detected in positive ion mode NAPA-LDI-MS analysis of organic phase serum extracts. CPA: cyclophosphatidic acid; LPA: lysophosphatidic acid; PA: phosphatidic acid; LPC: lysophosphatidylcholine; PC: phosphatidylcholine; LPE: lysophosphatidylethanolamine; PE: phosphatidylethanolamine; LPG: lysophosphatidylglycerol; DG: diacylglycerol; SM: sphingomyelin.

<i>m/z</i>	Assignment	Ion	Error (mDa)
258.1093	Glycerophosphocholine	[M+H] ⁺	-0.8
301.2104	Palmitic acid	[M+2Na-H] ⁺	-0.9
367.2832	Dihydroxyeicosanoic acid	[M+Na] ⁺	1.3
369.3505	Cholesterol	[M+H-H ₂ O] ⁺	-1.1
415.2205	CPA (16:0)	[M+Na] ⁺	-1.5
419.2543	CPA (18:1)	[M+H] ⁺	-1.4
437.2026	CPA (16:0)	[M+2Na-H] ⁺	-1.3
439.2199	CPA (18:2)	[M+Na] ⁺	-2.1
441.2361	CPA (18:1)	[M+Na] ⁺	-1.5
443.2522	CPA (18:0)	[M+Na] ⁺	-1.1
447.2852	LPA (18:0e)	[M+Na] ⁺	0.6
455.2118	LPA (16:0)	[M+2Na-H] ⁺	-2.7
457.2308	LPA (18:2)	[M+Na] ⁺	-1.7
459.2466	LPA (18:1)	[M+Na] ⁺	-1.6
461.2022	CPA (18:2)	[M+2Na-H] ⁺	-1.7
463.2182	CPA (18:1)	[M+2Na-H] ⁺	-1.4
469.2674	LPA (18:0e)	[M+2Na-H] ⁺	0.9
483.2465	LPA (18:0)	[M+2Na-H] ⁺	0.7
502.3274	LPC (P-16:0)	[M+Na] ⁺	0.6
506.3598	LPC (P-18:1)	[M+H] ⁺	-0.7
510.3538	LPE (20:0)	[M+H] ⁺	-1.6
518.3199	LPC (16:0)	[M+Na] ⁺	-1.9
524.3693	LPC (18:0)	[M+H] ⁺	-1.8
542.3201	LPC (18:2)	[M+Na] ⁺	-1.6
544.3357	LPC (18:1)	[M+Na] ⁺	-1.6
546.3513	LPC (18:0)	[M+Na] ⁺	-1.7
557.2832	LPG (18:0)	[M+2Na-H] ⁺	0.6
613.4786	DG (34:3)	[M+Na] ⁺	-1.6
637.4786	DG (36:5)	[M+Na] ⁺	-1.6
639.4951	DG (36:4)	[M+Na] ⁺	-0.8
665.5102	DG (38:5)	[M+Na] ⁺	-1.4
723.4922	PA (36:2)	[M+Na] ⁺	-1.3
725.5548	SM (d34:1)	[M+Na] ⁺	-2.0
745.4763	PA (36:2)	[M+2Na-H] ⁺	0.8
772.5832	PE (38:2)	[M+H] ⁺	-1.9
774.5983	PE (38:1)	[M+H] ⁺	-2.5

780.5493	PC (34:1)	$[M+Na]^+$	-2.0
782.5653	PC (34:1)	$[M+Na]^+$	-1.8
800.6147	PE (40:2)	$[M+H]^+$	-1.7
804.5497	PC (34:1)	$[M+2Na-H]^+$	0.7
806.5654	PC (36:3)	$[M+Na]^+$	-1.6
808.5807	PC (36:2)	$[M+Na]^+$	-2.0
832.5809	PC (38:4)	$[M+Na]^+$	-1.8

Table S6. Tentatively assigned ionic species detected in negative ion mode NAPA-LDI-MS analysis of organic phase serum extracts. LPA: lysophosphatidic acid; PA: phosphatidic acid; LPE: lysophosphatidylethanolamine; PE: phosphatidylethanolamine; LPI: lysophosphatidylinositol; PI: phosphatidylinositol; CerP: Ceramide phosphate; ST: sulfatide; PG: phosphatidylglycerol.

<i>m/z</i>	Assignment	Ion	Error (mDa)
209.0800	Azelaic acid	[M+Na-2H] ⁻	0.4
211.1344	Dodecanedioic acid	[M-H-H ₂ O] ⁻	1.0
227.2024	Myristic acid	[M-H] ⁻	0.7
241.0122	Inositol phosphate	[M-H-H ₂ O] ⁻	0.9
253.2180	Palmitelaidic acid	[M-H] ⁻	0.7
255.2337	Palmitic acid	[M-H] ⁻	0.7
259.0227	Inositol phosphate	[M-H] ⁻	0.2
269.2486	Heptadecanoic acid	[M-H] ⁻	0.0
279.2325	Linoleic acid	[M-H] ⁻	-0.4
281.2481	Oleic acid	[M-H] ⁻	-0.5
283.2637	Stearic acid	[M-H] ⁻	-0.6
295.2270	Hydroxyoctadecadienoic acid	[M-H] ⁻	-0.8
303.2324	Arachidonic acid	[M-H] ⁻	-0.6
305.2479	Eicosatrienoic acid	[M-H] ⁻	-0.7
327.2325	Eicosatrienoic acid	[M+Na-2H] ⁻	1.9
329.2480	Docosapentaenoic acid	[M-H] ⁻	-0.6
367.1590	Dehydroepiandrosterone sulfate	[M-H] ⁻	0.5
369.1746	Androsterone sulfate	[M-H] ⁻	0.4
377.2468	Tetracosahexaenoic acid	[M+Na-2H] ⁻	0.6
383.1537	Dihydroxyandrosthenone sulfate	[M-H] ⁻	0.3
391.2258	LPA (16:0)	[M-H-H ₂ O] ⁻	0.8
409.2367	LPA (16:0)	[M-H] ⁻	0.7
417.2419	LPA (18:1)	[M-H-H ₂ O] ⁻	1.3
419.2572	LPA (18:0)	[M-H-H ₂ O] ⁻	0.9
435.2524	LPA (18:1)	[M-H] ⁻	0.7
437.2683	LPA (18:0)	[M--H] ⁻	0.9
459.2532	LPA (18:0)	[M+Na-2H] ⁻	3.9
465.3056	Cholesterol sulfate	[M-H] ⁻	1.2
480.3106	LPE (18:0)	[M-H] ⁻	1.0
508.3418	LPE (20:0)	[M-H] ⁻	1.0
581.3113	LPI (18:0)	[M-H-H ₂ O] ⁻	2.2
598.4625	CerP (34:1)	[M-H-H ₂ O] ⁻	2.4
599.3215	LPI (18:0)	[M-H] ⁻	1.3
616.4731	CerP (34:1)	[M-H] ⁻	2.0
644.5063	CerP (36:1)	[M-H] ⁻	3.8
671.4672	PA (34:2)	[M-H] ⁻	1.4
673.4837	PA (34:1)	[M-H] ⁻	2.3

695.4671	PA (36:4)	$[M-H]^-$	1.3
699.4993	PA (36:2)	$[M-H]^-$	2.3
721.4828	PA (36:2)	$[M+Na-2H]^-$	3.8
726.5818	CerP (42:1)	$[M-H]^-$	1.1
742.5399	PE (36:2)	$[M-H]^-$	0.7
744.5558	PE (36:1)	$[M-H]^-$	0.9
766.5404	PE (38:4)	$[M-H]^-$	1.2
768.5567	PE (38:3)	$[M-H]^-$	1.8
770.5719	PE (38:2)	$[M-H]^-$	1.4
778.5158	ST (34:1)	$[M-H]^-$	1.4
794.5105	PE (42:9)	$[M-H-H_2O]^-$	-1.9
795.5151	PG (36:2)	$[M+Na-2H]^-$	-0.6
885.5504	PI (38:4)	$[M-H]^-$	0.5

REFERENCES

(1) Psychogios, N.; Hau, D. D.; Peng, J.; Guo, A. C.; Mandal, R.; Bouatra, S.; Sinelnikov, I.; Krishnamurthy, R.; Eisner, R.; Gautam, B.; Young, N.; Xia, J. G.; Knox, C.; Dong, E.; Huang, P.; Hollander, Z.; Pedersen, T. L.; Smith, S. R.; Bamforth, F.; Greiner, R.; McManus, B.; Newman, J. W.; Goodfriend, T.; Wishart, D. S. *Plos One* **2011**, *6*, e16957.